Dynamics of Ionic and Cytotoxic Edema During Acute and Subacute Stages of Patients With Ischemic Stroke: Complementarity of 23Na MRI and Diffusion MRI

Maëva Cotinat, Noëlle Messaoudi, Emmanuelle Robinet, Laurent Suissa, Emilie Doche, Maxime Guye, Bertrand Audoin, Laurent Bensoussan, Jean-philippe Ranjeva, Wafaa Zaaraoui

NMR in Biomedicine

WILEY

NMR IN BIOMEDICINE

RESEARCH ARTICLE OPEN ACCESS

Dynamics of Ionic and Cytotoxic Edema During Acute and Subacute Stages of Patients With Ischemic Stroke: Complementarity of ^{23}Na MRI and Diffusion MRI

Maëva Cotinat[1,2,3] | Noëlle Messaoudi[4] | Emmanuelle Robinet[4] | Laurent Suissa[4,5] | Emilie Doche[4,5] | Maxime Guye[1,2] | Bertrand Audoin[2,6] | Laurent Bensoussan[7] | Jean-Philippe Ranjeva[1,2] | Wafaa Zaaraoui[1,2]

[1]Aix Marseille Univ, CNRS, CRMBM, Marseille, France | [2]Aix Marseille Univ, APHM, Timone, CEMEREM, Marseille, France | [3]Physical and Rehabilitation Medicine Department, Aix Marseille Univ, APHM, Hôpitaux Sud, Marseille, France | [4]Neurovascular Department, Aix Marseille Univ, APHM, Timone, Marseille, France | [5]Aix Marseille Univ, INSERM, CR2VN, Marseille, France | [6]Neurology Department, Aix Marseille Univ, APHM, Timone, Marseille, France | [7]Physical and Rehabilitation Medicine Department, Aix Marseille Univ, APHM, INT, Hôpitaux Sud, Marseille, France

Correspondence: Maëva Cotinat (maeva.cotinat@ap-hm.fr)

Received: 11 December 2024 | **Revised:** 4 March 2025 | **Accepted:** 5 March 2025

Funding: This work was supported by France Life imaging; Agence Nationale de la Recherche France 2030.

Keywords: edema | MRI | sodium | ^{23}Na MRI | stroke

ABSTRACT

Cerebral imaging is crucial in the diagnosis and treatment algorithm of acute stroke to determine salvageable brain tissue. While diffusion MRI is commonly used to define the ischemic core, it cannot reliably distinguish irreversibly damaged from salvageable tissue. We investigated the added value of ^{23}Na MRI to define irreversible necrotic tissue after a stroke. Fifteen patients with acute stroke involving medial cerebral artery occlusion were longitudinally explored with conventional and ^{23}Na MRI within 24 h, 70 h following stroke and at 3 months to characterize the necrotic area. Time-courses of sodium accumulations were observed within regions presenting with or spared by cytotoxic/ionic edema and converting or not to necrosis. Dynamics of sodium accumulations were very different across subjects. At the group level, time-courses of sodium signal in cytotoxic edema showed a non-linear increase with an upper asymptote of 59 ± 6%% relative to the contralateral hemisphere. Regions with a larger early increase in ^{23}Na signal (ionic edema) showed a non-linear accumulation during the first 70 h and were associated with subsequent necrosis at month 3. Some of the regions with no ionic edema during the first 70 h became necrotic at month 3, showing that pejorative pathophysiological processes could worsen after 70 h following attack. Final necrotic volume was well predicted by the cytotoxic volume (ADC decrease) during the first 24 h, and by the volume of ionic edema during the subacute period (25–70 h) following attack. The regions showing ionic edema showed a non-linear increase of ^{23}Na signal during the first 70 h, with larger sodium accumulations in regions converting to necrosis at month 3. It may be of interest to consider the role of ionic edema imaging in the 70 h after stroke and reperfusion, with a view to better understand stroke pathophysiology. Sodium MRI could add complementary information about the fate of cell necrosis within low ADC signal regions.

Abbreviations: NIHSS, National Institutes of Health Stroke Scale; ROI, Region of interest; DWI, Diffusion-weighted image; ADC, Apparent diffusion coefficient.

1 | Introduction

Stroke is the leading cause of mortality and morbidity worldwide. Acute ischemic stroke is caused by an abrupt reduction in blood flow within specific brain areas, which induces a sequence of neurochemical processes known as the ischemic cascade leading to tissue necrosis when therapeutic interventions are not efficient [1]. Although cerebral imaging is pivotal in the diagnosis and treatment planning of stroke, the major challenge during the acute phase is identifying salvageable tissues. The core identified on early computed tomography (CT) or magnetic resonance imaging (MRI) does not represent tissue that is already infarcted but "rather a probabilistic estimate of tissue that is highly likely to become infarcted, if fast reperfusion does not occur" [2]. The most commonly used MRI sequence to define the ischemic core is diffusion. Diffusion-weighted imaging (DWI) identifies cytotoxic edema through the limited motion of water molecules in the extracellular space [3]; thus, a high DWI signal does not necessarily represent irreversibly infarcted tissue [4]. Regions with low apparent diffusion coefficient (ADC) have been demonstrated to represent the most reliable imaging marker for infarct core assessment [5]; however, it does not accurately differentiate irreversibly damaged ischemic from salvageable tissue [6].

As the definition of core areas was based on metabolism [6], imaging more directly metabolic and ionic homeostatic changes should facilitate the therapeutic decision. Thus, MRI can study sodium levels of tissues non-invasively [7]. Some authors have proposed that ^{23}Na MRI could provide clinicians with additional insight into the individual metabolic status [8]. Wetterling et al. [9] preclinical study's suggested that sodium-MRI in conjunction with ADC can serve as a viability marker in order to facilitate time-independent assessment of tissue fate and cellular bioenergetics failure in stroke patients. In a clinical cross-sectional study, Tsang et al. [10] demonstrated that the signal intensity of sodium increased in a time-dependent manner during acute ischemic stroke in humans, whereas the ADC of water did not provide any useful temporal information while reaching a plateau. In line with these results, Hussain et al. [11] modeled the non-linear increase in sodium signal intensity within the cytotoxic edema (defined by the region of decreased ADC) with a sigmoid curve which showed an initial slow ramp-up lasting 5 to 6 h, followed by a more rapid increase between 18 and 20 h to finally reach an upper asymptote around +70% for sodium intensity within the cytotoxic edema relative to the normal contralateral hemisphere. However, this cross-sectional study did not account for potential interindividual differences and did not provide any prognostic values for ^{23}Na MRI to define irreversible necrotic tissue.

Recent studies have highlighted the significant challenge posed by infarct expansion despite successful recanalization in acute ischemic stroke patients, underscoring the potential utility of MRI in evaluating post-reperfusion injury [12, 13]. The reperfusion benefit may be independent of current imaging constructs and this also question the accuracy and utility of conventional imaging modalities in defining reversible versus irreversible ischemia [14]. In this context, alternative MR methods like ^{23}Na MRI may provide novel insights into cellular and metabolic dynamic after reperfusion, offering a complementary approach to conventional MRI for post-treatment evaluation of tissue viability. To address these points, we conducted a longitudinal follow-up study in 15 patients with acute stroke explored with conventional proton MRI and ^{23}Na MRI at different time points: (i) within the first 24 h following onset, (ii) within the first 70 h, and finally (iii) 3 months after the stroke event with only conventional MRI to characterize the necrotic area. We aimed to confirm the dynamics of ^{23}Na concentrations in cytotoxic edema defined by low ADC, and to characterize the dynamics of ^{23}Na and ADC signals within areas showing abnormal ^{23}Na signal, abnormal ADC, final necrotic tissue, and various overlays of these regions in order to better understand the tissue evolution after stroke recanalization. Finally, we examined the inter-individual differences in the dynamics of cellular and ionic parameters across these areas to assess the potential individual value of this modality.

2 | Experimental

2.1 | Participants and Clinical Assessment

This study was conducted at the University Hospital of Marseille (AP-HM), France, following the approval of the local ethics committee (CPP Sud Méditerrannée V, 2014-A01532-45). Individuals were included in the study after obtaining verbal and written informed consent.

Adults with hemispheric ischemic stroke with a definite time of onset less than 24 h, stroke volume greater than 1.5 mL on the clinical MRI performed prior to the revascularization therapy, no history of neurological or psychiatric pathology, and no contraindication to MRI were included in the study. Exclusion criteria included the usual contraindications to MRI, risk of noncompliance, unstabilized neurological or hemodynamic state. All subjects received standard care, including intravenous thrombolysis if indicated. ^{23}Na and ^{1}H MRI were performed within 24 h of the stroke, then between 25 and 70 h. Then, at 3 months, only conventional MRI with fluid-attenuated inversion recovery (FLAIR) and 3D-T1-weighted Magnetization Prepared RApid Gradient Echo (MPRAGE) were performed. Clinical assessment was performed by an expert neurologist, including the National Institutes of Health Stroke Scale (NIHSS) score at each time point and the Rankin score [15] measured 3 months after attack [16].

2.2 | MRI Data Acquisition

MR imaging was performed on a 3 T Verio system (Siemens Healthineers, Erlangen Germany) equipped with multi-nuclear options, using a double tuned ^{23}Na-^{1}H volume head coil (Rapid Biomedical, Rimpar, Germany).

The ^{1}H MRI protocol included a 2D FLAIR sequence (TE/TR/TI = 95/9000/2500 ms, 24 slices with 10% slice gap, voxel size = 0.9 × 0.9 × 5 mm, FOV = 240 mm, acquisition time = 4 min 14 s), a 3D-T1-weighted MPRAGE sequence (TE/TR/TI = 3.41/1900/900 ms, voxel size = 0.9 × 0.9 × 0.9 mm, FOV = 230 mm, acquisition time = 5 min 53 s) and an axial

diffusion-weighted echo planar imaging sequence (TE/TR = 152/6700 ms, 24 slices with 10% slice gap, voxel size = 1.3 × 1.3 × 5 mm, FOV = 240 mm, b0 and b = 1000 s/mm^2, 3 directions, acquisition time = 1 min 55 s).

The ^{23}Na MRI acquisition consisted in a 3D density-adapted radial projection reconstruction pulse sequence [17] (TE = 200 μs, TR = 100 ms, 6000 projections, with 384 data points each, flip angle = 90°, pulse length = 0.320 ms, gradient amplitude = 4.6 mT/m, readout duration = 20 ms, nominal spatial resolution of 4 × 4 × 4 mm^3, 10 min of acquisition time).

2.3 | Data Processing

Reconstruction of the 3D radial sodium acquisition was performed offline using a home-made procedure developed on Matlab (R2011b, MathWorks) [17]. Rician noise was removed by using a nonlocal means denoising filter on the reconstructed 3D data [18].

2.3.1 | Definition of the Regions of Interest

The definition of lesional ROIs was conducted manually independently by two experienced operators (NM, MC) using the FSLVIEW platform for each image type and time point. This was performed on coregistered images to ensure spatial consistency across modalities and time points. The lesional ROIs were delineated as regions showing hypersignals on Na MRI, b1000 diffusion weighted MRI and FLAIR). Hypersignal was defined as brain areas that exhibit higher signal intensities compared to surrounding tissues and to contralateral region as described in previous studies [7, 19–21]. All regions appearing as hyperintense compared to the contralateral side were included in the delineation, with heterogeneous areas within the lesion being preserved as part of the ROIs. Both operators analyzed the entire dataset, and very strong correlations were observed between the lesion volumes delineated by the two operators. To minimize the risk of bias and variability inherent to manual contouring, we averaged the values obtained from the two operators. At each time point, the contralateral zones were defined by flipping the 'lesion' contour after registration on brain templates for ^{23}Na and diffusion-weighted images. The ^{23}Na, FLAIR, and diffusion-weighted images were aligned onto high-resolution ^{1}H images (MPRAGE) at each time point. MPRAGE images at time points 1 and 2 were coregistered with the high-resolution MPRAGE images at 3 months to allow registration of the other sequences. Thus, the "early ionic edema" was defined as the region characterized by hypersignal observed on ^{23}Na maps during the first 70 h, the "early cytotoxic edema" as the region characterized by hypersignal observed on b1000 images during the first 70 h and the "necrosis" as the region characterized by hypersignal observed on FLAIR at 3 months. To better characterize the dynamics of the different pathological processes occurring during the first 70 h following attack, we also characterized the regions of 'early ionic edema converting to necrosis' (ROI HighNa∩FlairM3), "necrotic region not exhibiting early ionic edema" (ROI FlairM3 minus HighNa), "early cytotoxic edema converting to necrosis" (ROI lowADC∩FlairM3), "necrotic region not exhibiting early cytotoxic edema" (FlairM3 minus lowADC), and "early ionic edema not converting to necrosis" (ROI HighNa minus FLAIR). A schematic representation of the regions of interest and their definitions is provided in Figure 3A,B. Mean values (^{23}Na signal and ADC) were extracted from the different ROIs and their contralateral analogues before computing the percentage signal changes: (signal intensity$_{ipsi}$ - signal intensity$_{contra}$)/signal intensity$_{contra}$ × 100.

2.4 | Statistics

A non-linear sigmoid fit ($f(t) = \frac{\alpha * t^{\delta}}{e^{\gamma} + t^{\delta}}$) was applied to the 28 relative sodium signal intensity data points collected over the 70 h following stroke onset [11].

Moreover, we displayed the evolution of the time courses observed in different regions of interest by pooling all subjects and their individual longitudinal data with a local linear fit representation. Temporal dynamics of the ^{23}Na signal and ADC between the different regions exhibiting different pathophysiological processes and prognoses were compared using paired ANOVA at the group level. We conducted a nonparametric correlation analysis using Spearman's correlation coefficients.

For all statistical tests, a significance level of $p < 0.05$ was employed.

3 | Results

A total of 15 participants were enrolled in the study. One patient showed cytotoxic edema volume less than 1 mm^3. In order to limit the effect of partial volume effect, we excluded this patient. In total, 14 patients were analyzed seven females and eight males. The mean age of the participants was 68 ± 13 years. The means NIHSS at admission was 10 ± 6 and 5 ± 4 at the first MRI of this study, after recanalization. The NIHSS at admission and at the MRI time points are shown in Table 1. In our study, 60% of the subjects experienced an ischemic stroke due to involvement of the left middle cerebral territory while 27% had right middle cerebral territory involvement. A total of 13 subjects received intravenous thrombolysis as part of their treatment and 3 subjects underwent thrombectomy.

A total of 28 time points were recorded over the first 3 days following the stroke event. Details of the participant characteristics are presented in Table 1.

Figure 1 presents representative MR images from the 15 subjects, scanned prior to 24 h after the onset of stroke and again within 3 days. These data show different dynamics of increase in the ^{23}Na signal with time after the onset for each individual. The diffusion sequence from one subject (P10) and the MPRAGE of another (P13) were not analyzable due to the presence of movement artifacts. Two subjects were unable to undergo scanning between 24 and 70 h due to a clinical aggravation that was incompatible with MRI scanning (P4 and P13).

TABLE 1 | Stroke individuals characteristics.

Patient no.	Age (year)	Sex	Acute stroke treatment	Vascular territory, clot location	NIHSS Initial/first acquisition/ second acquisition	Time of serial MRI (h)	DWI initial lesion volume (cm^3)
P1	57	M	IV tPA	Left MCA, M2	24/17/16	17.4/64.4	87.7
P2	64	M	IV tPA	Right MCA, ICA	6/4/0	22/69	83.3
P3	87	F	IV tPA	Left MCA, M2	11/8/1	6.2/51.5	19.2
P4	67	M	IV tPA + MT	Left MCA, M1	22/11/–	24.7	31.9
P5	40	M	IV tPA	Left MCA, ACI	10/3/2	15.3/37.7	20.3
P6	70	F	IV tPA + MT	Right MCA, M1	15/3/2	13.5/63.2	7.7
P7	49	M	IV tPA	Left MCA, M2	13/1/1	21.5/43.2	3.0
P8	70	F	IV tPA	Right MCA, NV	9/1/1	20.5/67.4	11.1
P9	71	M	IV tPA	Left PCA, NV	10/8/2	20.5/46.5	1.6
P10	87	F	IV tPA	Left MCA, M1	9/8/5	24.5/68.8	7.4
P11	75	F	IV tPA	Left MCA, M3	6/3/2	18.5/65	1.7
P12	65	M	IV tPA + MT	Left MCA, M1	6/0/0	16.8/40.5	3.2
P13	84	F	IV tPA	Right MCA, M1	8/2/–	16	1.4
P14	69	M	None	Left MCA, NV	3/3/0	3.8/75	1.3

Abbreviations: DWI, diffusion-weighted imaging; ICA, internal carotid artery; IV tPA, intravenous tissue plasminogen activator; MCA, middle cerebral artery; MRI, magnetic resonance imaging; MT, mechanical thrombectomy; NIHSS, National Institutes of Health Stroke Scale; NV, not visible; PCA, posterior cerebral artery.

3.1 | Cellular and Ionic Dynamics of the Region Involved by Early Cytotoxic Edema

By fitting all experimental data points during the first 70 h in the region of cytotoxic edema (region characterized by abnormal low ADC values), the dynamics of ^{23}Na MRI followed a sigmoid curve (RMSE = 15.8; $\alpha = 91 \pm 108$, $\delta = 0.71 \pm 0.9$, $\gamma = 2.3 \pm 0.8$) of increases in signal intensity with an upper asymptote reaching +59% (±6%) (adjusted standard deviation) compared to the normal contralateral hemisphere (Figure 2A). Concurrently, the drop in ADC values reached rapidly a plateau of low ADC (around −45% relative to the contralateral side) during this period (Figure 2B).

3.2 | Cellular and Ionic Dynamics of Regions Affected by the Different Pathophysiological Processes or Prognoses

Figure 3 shows the temporal evolution of the regions defined in accordance with the pathophysiological processes observed over the first 70 h and tissular prognosis at 3 months.

3.3 | Ionic Edema

The regions showing ionic edema (i.e., ROI with observable ^{23}Na signal increase) showed a non-linear increase of ^{23}Na signal during the first 70 h, with faster and larger sodium accumulations in regions showing "ionic edema in the first 70 h converting to necrosis" compared to the global ionic edema and regions "without early ionic edema but converting to necrosis at 3 months" (Figure 3). Paired-ANOVA comparing sodium accumulations between ROIs ("ionic edema," "ionic edema converting to necrosis," "necrosis without early ionic edema," and "ionic edema not converting to necrosis") using time as variable showed a significant global effect ($F(1, 31) = 2.319$, $p < 0.0001$), a significant time effect ($p < 0.0001$) and a significant ROI × time interaction during the first 70 h following stroke onset ($p > 0.0001$). Post hoc tests showed that sodium accumulations were significantly different between the ROIs sorted by decreasing order of Na signal increase:

"ionic edema converting to necrosis" > "ionic edema" > "'ionic edema not converting to necrosis" > "necrosis without early ionic edema."

3.4 | Cytotoxic Edema

Less dynamics were observed in cytotoxic edema, with a plateau of low ADC signal (around −45% relative to the contralateral side) during this period. Paired-ANOVA comparing ADC decreases within ROIs ("cytotoxic edema," "cytotoxic edema converting to necrosis," "necrosis without early cytotoxic edema," and "cytotoxic edema not converting to necrosis") using time as variable showed a significant global effect ($F(3,35) = 4.673$, $p < 0.008$), a significant time effect ($p < 0.0001$) and a significant ROI × time interaction during the first 70 h following stroke onset ($p < 0.008$).

Post hoc tests showed that ADC decreases were significantly different between the ROIs with ADC values of regions with:

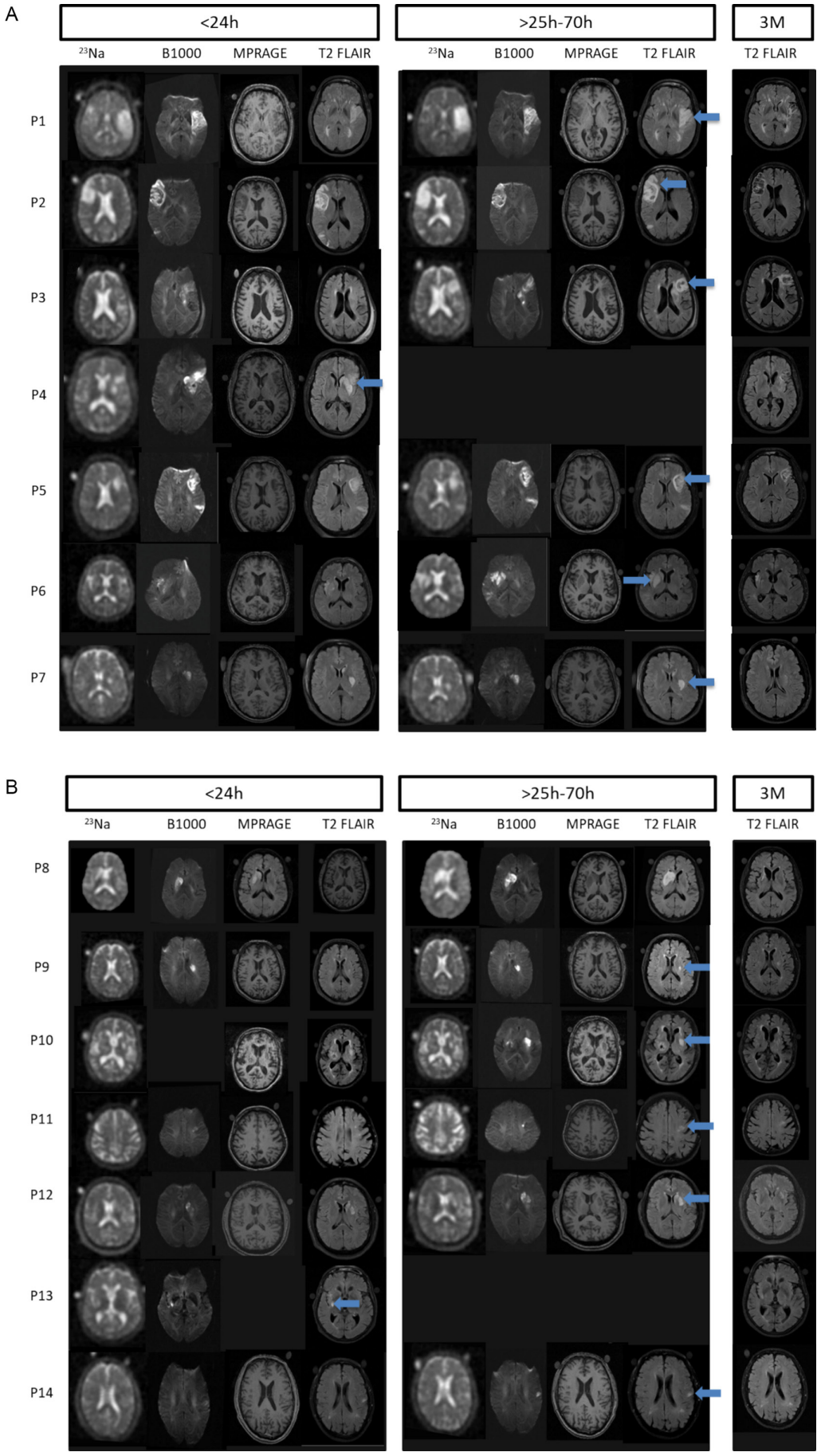

FIGURE 1 | Legend on next page.

FIGURE 1 | Representative MRI images from the 15 patients with ischemic stroke explored during the acute and subacute phases and at 3 months. The arrows indicate the stroke lesion. The subjects were ranked in descending order of the volume necrosis at 3 months.

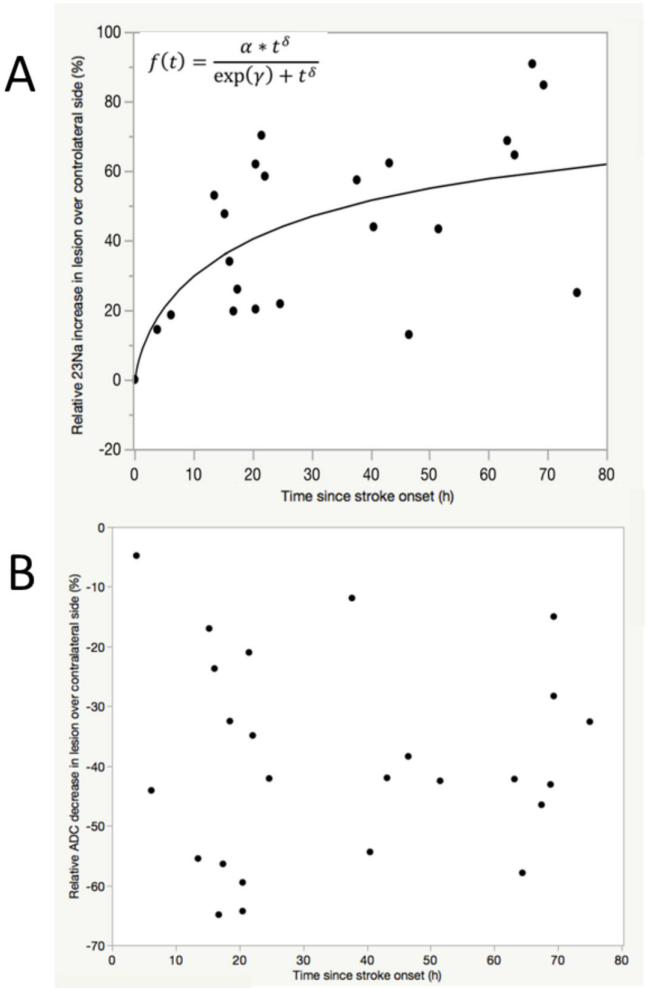

FIGURE 2 | Dynamics of (A) ^{23}Na and (B) ADC signals during the first 70 h following ischemic stroke. (A) Relative sodium intensity increases non-linearly over time during the first 70 h after stroke onset ($n = 28$; RMSE = 15.8; $\alpha = 91 + 108$, $\delta = 0.71 + 0.9$, $\gamma = 2.3 + 0.8$), while (B) a plateau of low ADC is reached during the first hours following attack.

"cytotoxic edema converting to necrosis" < "cytotoxic edema" < "cytotoxic edema not converting to necrosis" < "necrosis without early cytotoxic edema."

3.4.1 | Volume Necrosis Prediction

During the first 24 h following stroke (Figure 4B), the volume of ionic edema was statistically smaller than those of cytotoxic edema ($p < 0.001$) and those of the final necrotic area at 3 months ($p = 0.002$) while the volume of the cytotoxic area was not statistically different from those of the final necrotic area ($p = 0.502$).

During the 24–70 h period following attack, the volume of ionic edema was not different than those of the final necrotic area ($p = 0.519$), while the volume of cytotoxic edema was significantly larger relative to ionic edema ($p = 0.002$) and final necrotic area at 3 months ($p = 0.002$).

During the 70 h following the stroke event, the increase of ^{23}Na signal was significantly correlated with the necrosis volume at 3 months ($\rho = 0.662$, $p = 0.002$) (Supplementary material 1). The decrease in ADC signal showed a very weak and non-significant correlation with the necrosis volume at 3 months ($\rho = 0.279$, $p = 0.159$). The decrease in ADC signal and the increase of ^{23}Na signal showed a weak and non-significant correlation ($\rho = 0.114$, $p = 0.615$). The volume of ionic and cytotoxic edema were respectively significantly correlated with the necrosis volume at 3 months (respectively $\rho = 0.837$, $p < 0.001$, and $\rho = 0.890$, $p < 0.001$) (Supplementary material 1).

Non-parametric correlation analyses (Spearman rank) showed no correlation between the NIHSS, necrosis at month 3, the volumes of cytotoxic, and ionic edema. However, significant correlations were observed between volume of necrosis at month 3 and the volumes of cytotoxic and ionic edema during the first 70 h following stroke (Spearman coefficient 0.8, $p < 0.001$). Additionally, we found a moderate correlation between the volume of necrosis at month 3 and the lesional high sodium signal intensity (Spearman coefficient 0.5, $p = 0.02$). However, no significant correlation was observed between the lesional high sodium signal intensity and lesional low ADC, nor between the lesional low ADC and necrosis volume at month 3.

3.4.2 | Inter-Individual Variability

Dynamics of ^{23}Na signal intensities and ADC values within ionic and cytotoxic edema were variable across individuals during the first 70 h following stroke onset, both in terms of asymptotic values of ^{23}Na signals ([(0%)-(+120%)], or plateau for the decrease of ADC ([(−10%)-(−75%)] (Figure 5). Such inter-subject variability was also observed for the volumes of ionic edema, cytotoxic edema and final necrosis (Figure 4A,B).

4 | Discussion

The objective of this study was to use in vivo MRI to investigate the degree of dyshomeostasis and cytotoxic damage known to occur in the first 70 h after stroke onset. The dynamics of ionic and cytotoxic edema were very different across subjects. Our data confirmed previous findings [11, 22], demonstrating at the group level that ^{23}Na signal intensity increases in a sigmoid time-dependent manner after ischemic stroke onset in humans, whereas ADC variations exhibited smaller dynamics during this period, reaching a plateau few hours after onset [11]. Regions with a larger early increase in ^{23}Na signal (ionic edema) showed a non-linear accumulation during the first 70 h and were associated with subsequent necrosis at month 3. The final necrotic

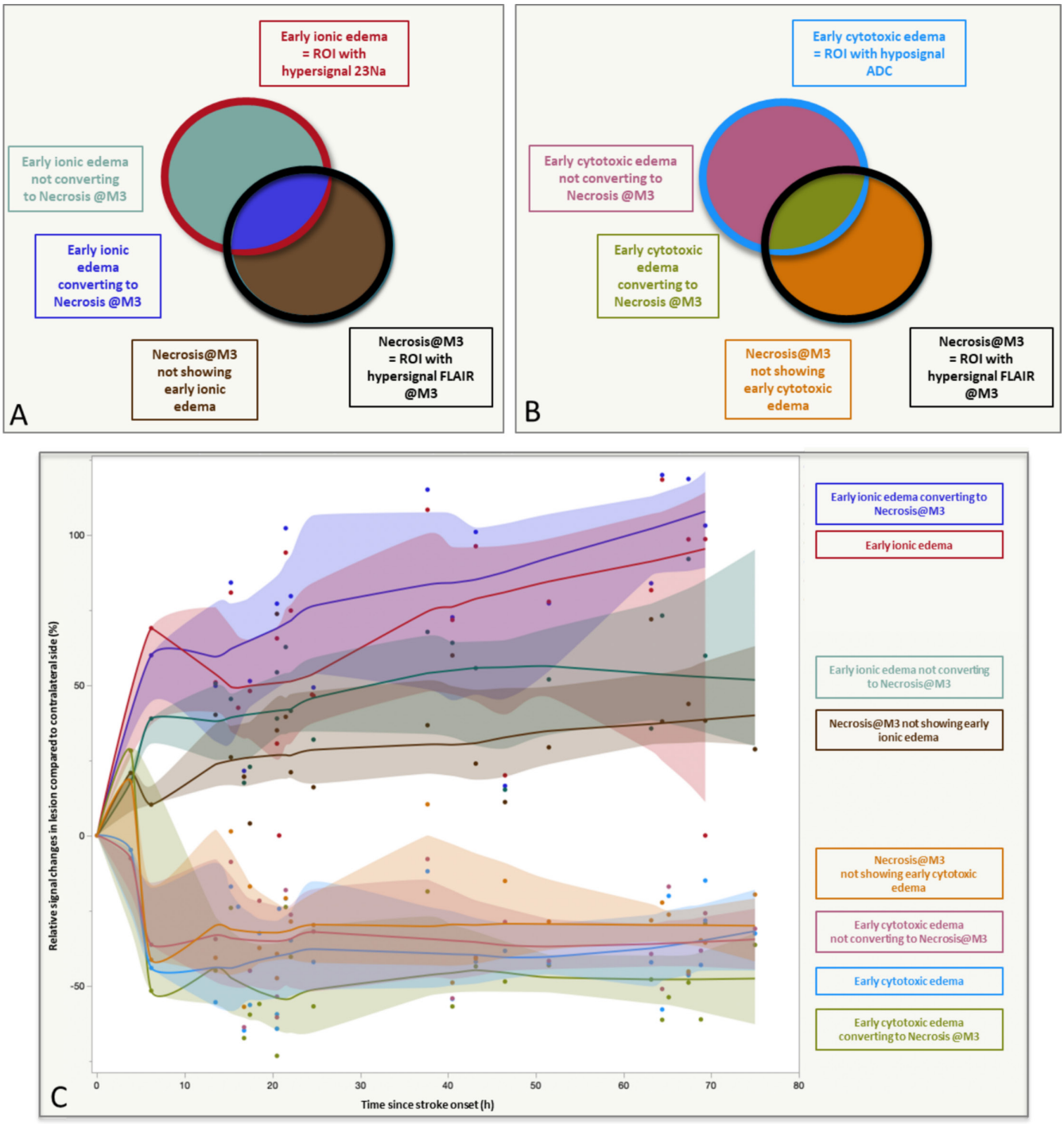

FIGURE 3 | Dynamics of ^{23}Na accumulations and low ADC in acute and subacute stages of ischemic stroke. (A) This figure depicts the regions of interest (ROIs) identified on the hyperintense ^{23}Na (red circle) and hyperintense FLAIR (black circle) sequences. The intersections between these ROIs (overlapping areas) and the regions exclusive to each ROI are highlighted to facilitate visualization of the data presented in (A). (B) This figure depicts the regions of interest (ROIs) identified on the hypointense ADC (light blue circle) and hyperintense FLAIR (black circle) sequences. The intersections between these ROIs (overlapping areas) and the regions exclusive to each ROI are highlighted to facilitate visualization of the data presented in (A). (C) Curves represent the relative variations of ^{23}Na and ADC in lesions compared to homologous contralateral regions. The dynamics of regions showing different long-term prognosis (necrosis or recovery), and different early pathophysiological processes (ionic edema, cytotoxic edema, no edema) are compared. @M3, at 3 months.

volume at Month 3 was well predicted by the volume of cytotoxic edema observed during the first 24 h. However, during the subacute period, 25–70 h following attack, the volume of ionic edema was the best predictor of the final necrotic volume of necrosis at month 3.

Following stroke, the rapid depletion of substrates for energy production results in the reduction of the production of adenosine triphosphate, the accumulation of lactate via anaerobic glycolysis and energy failure. One consequence is the dysfunction of the Na^+/K^+-ATPase pumps, which is responsible for ionic

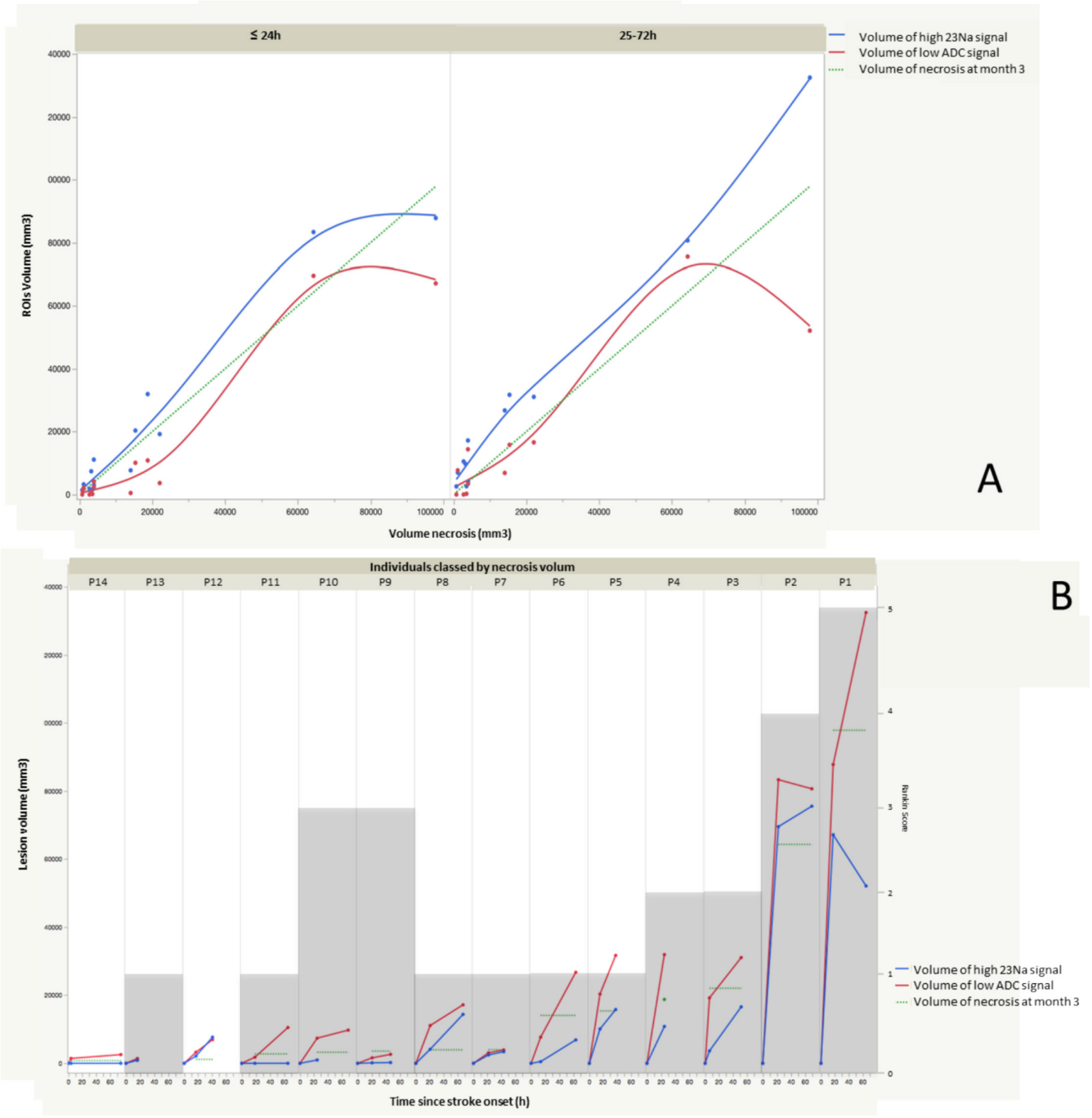

FIGURE 4 | volumes of cytotoxic and ionic edema during the acute and subacute phases. (A) Subject-wise volume dynamics of cytotoxic (red) and ionic (blue) edema compared to final volume of necrosis at 3 months (green). (B) The better prediction of final necrotic volume by cytotoxic edema during the first 24-h period (left) while ionic edema predicts better necrosis at 3 months during the subacute period (right).

edema, as evidenced by increases in intracellular levels of Na^+ and extracellular levels of K^+. The depletion of energy reserves leads to depolarization in neurons and glia, caused by the loss of membrane potential [23]. The depolarization triggers the rapid release of excitotoxic amino acids, mainly glutamate, into the extracellular space at the beginning of ischemia. Apart from the direct neurotoxic effects of glutamate on neurons, the activation of glutamate receptors has been proven to elevate intracellular levels of Ca^{2+}, Na^+, and Cl^-. This, in turn, has been demonstrated to induce cytotoxic edema and oxidative stress through the generation of free radicals and the subsequent activation of related enzymes, ultimately resulting in necrosis and apoptosis [1]. Subsequently, cytotoxic edema and events driven by excessive intracellular Ca^{2+} reach their peak approximately 24 h after the onset of the attack [24]. The blood–brain barrier is affected by ischemic stroke in a two-phase process. In the initial 2-h period following the ischemic event, damage to the endothelial basal lamina results in an increased permeability of the blood–brain barrier. The second phase, occurring between 24- and 72-h post-infarction, is distinguished by leukocyte infiltration, which results in additional tissue damage. The compromised blood–brain barrier enables the leakage of

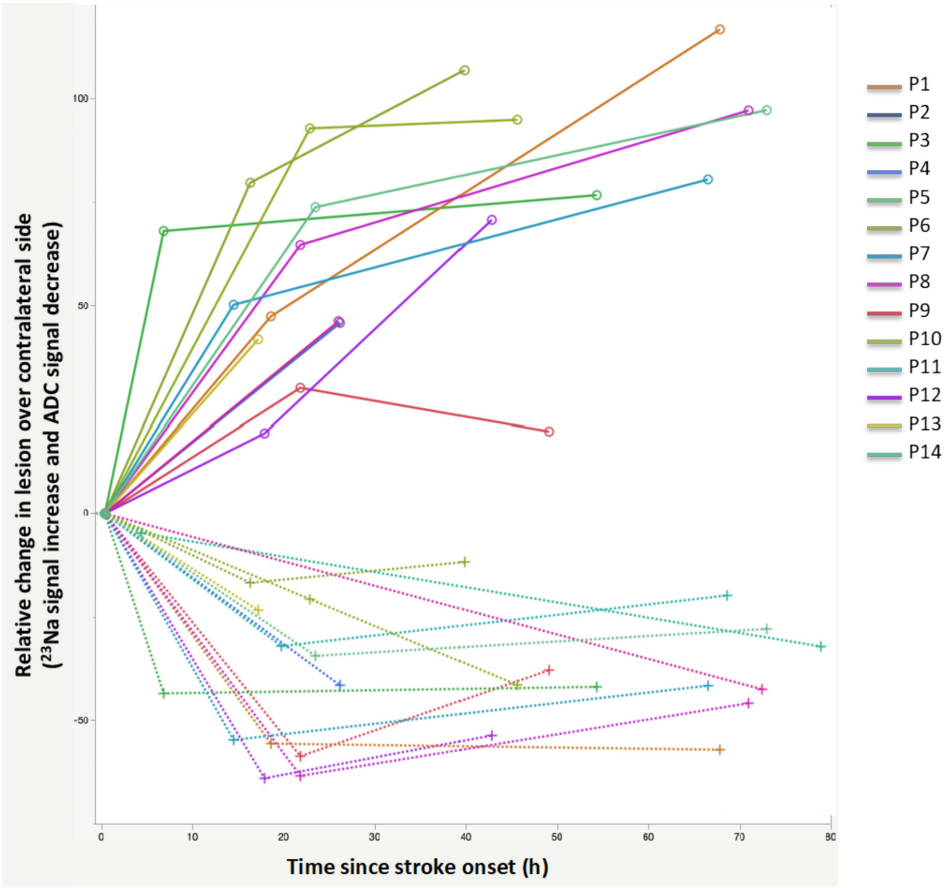

FIGURE 5 | Inter-individual heterogeneity in the dynamics of ^{23}Na accumulations and ADC decreases in stroke patients.

high molecular weight molecules and water, resulting in the formation of vasogenic edema. This effect reaches its maximum intensity 3 to 5 days after the onset of ischemia and can persist for days to weeks [24]. Despite substantial research efforts and considerable advancements in our understanding of stroke pathophysiology, the therapeutic options for acute stroke remain notably constrained. While thrombolysis and thrombectomy have demonstrated effectiveness in the management of ischemic stroke, additional research is required to enhance clinical outcomes and reduce the risk of complications [25]. Recent studies have emphasized the substantial challenge of infarct expansion despite successful recanalization in patients with acute ischemic stroke, highlighting the potential role of MRI in assessing post-reperfusion injury [12, 13]. Notably, the benefits of reperfusion may occur independently of conventional imaging modalities, raising questions about the accuracy and utility of conventional imaging techniques in distinguishing reversible from irreversible ischemia [14]. Alternative MR methods, such as ^{23}Na MRI may offer novel insights into cellular and metabolic dynamics following reperfusion, providing a complementary tool to conventional MRI for evaluating tissue viability after treatment. Advancing knowledge of stroke pathophysiology seems crucial for integrating new therapeutic approaches, including neuroprotective agents [26].

The analysis of different regions of interest based on their necrotic outcome at month 3 revealed areas exhibiting a ^{23}Na hypersignal, indicating a disturbance in sodium homeostasis in the first 70 h following stroke. However, parts of brain regions showing ionic edema during the acute and subacute phases did not progress to necrosis at Month 3, likely due to effective reperfusion mechanisms. Conversely, some areas that became necrotic at Month 3 did not exhibit any significant increases in the ^{23}Na signal during the first 70 h. These results suggest that ionic edema may continue to progress beyond 70 h after stroke onset, aligning with observations from middle cerebral artery occlusion models in rats, which showed peak sodium concentrations at 72 h and sustained elevated sodium levels for up to 3 to 6 weeks [27, 28]. These results, obtained in rats after permanent occlusion of the middle cerebral artery, are supported in particular by an ischemia–reperfusion study which found an inverse correlation between Na+/K+-ATPase activity and the volume of ischemic lesion and clinical score [29]. Huang et al. found a progressive reduction in Na+/K + ATPase activity at 6 h, 24 h and 48 h, which persisted for up to 7 days and was inversely correlated with the increase in infarct volume, which progressively increased for up to 7 days [29].

Recent literature highlights the limitations of utilizing ADC to define the ischemic core and assess tissue recovery in the acute phase following a stroke [6, 30]. Investigating whether sodium MRI could aid in delineating tissue fate would be of interest. It appears plausible that sodium imaging could provide supplementary information beyond that obtained from routinely employed sequences. This study confirmed that the necrotic volume at 3 months could be predicted by the volume of brain region with low ADC within the first 24 h [31], but not during the subacute phase. Interestingly, between 25 and 70 h following

attack, the volume of brain region exhibiting ^{23}Na hypersignal predicted well the final necrotic volume. Moreover, this study demonstrated that combining diffusion and ^{23}Na MRI may better characterize the pathophysiological dynamics of stroke up to 80 h after attack. In the present study, this approach was used to differentiate between regions susceptible to become necrotic at month 3. Sodium MRI may offer valuable insights into the sub-acute phase of stroke, providing additional information on tissue viability in regions with cytotoxic edema and delayed sodium metabolism changes.

Although the accumulation of unsuccessful results in the clinical translation of neuroprotective treatments for stroke has tempered expectations in recent years, advances in and the growing use of recanalization therapies have rekindled optimism in the field of neuroprotection [32]. Administering neuroprotective drugs after successful reperfusion appears crucial for direct protection of the ischemic penumbra [32]. Multimodal imaging techniques can provide valuable insights into the pathophysiology of stroke and potentially help to clarify the role of neuroprotective agents. Notably, our study identified regions with disturbed ^{23}Na homeostasis in the subacute phase that did not progress to necrosis, as well as others that became necrotic at month 3. This suggests that the fate of these regions is not fixed and that further interventions, such as neuroprotection, could help preserve these vulnerable regions and prevent their progression to necrosis.

Concurrently, our study highlights the existence of a significant degree of inter-individual heterogeneity within the cohort, which limits the translation of the results into general clinical practice. A deeper understanding of tissue phenomena following stroke will necessitate an individualized approach in future studies. Variability among ischemic stroke individuals may be attributed to factors such as lesion location, stroke etiology, distribution of gray and white matter tissue and the extent of perfusion deficits or reperfusion. In addition, the low-resolution images generated by ^{23}Na MRI restrict precise segmentation of smaller lesions [33].

This study is subject to some limitations, including the relatively small number of subjects and the heterogeneity of the population, which may affect the generalizability of the findings. Additionally, to ensure no delay or missed opportunities for ischemic stroke treatment, the imaging procedures described in this research protocol were conducted only after clinical imaging and any reperfusion treatments were completed. In addition, the low spatial resolution of in vivo sodium MRI can contribute to PVE, particularly in small ROIs. Thus, here with a nominal resolution of 4 mm isotropic voxel (nominal voxel volume 0.064 cm^3) and when accounting for the point spread function, the ^{23}Na MRI acquisition had a real voxel volume of approximatively 0.2 cm^3. To minimize the effect of PVE due to mixed tissue signals, we ensured that all ROIs studied had a volume superior to 1 cm^3, representing at least 5 voxels of the ^{23}Na MRI acquisition. Additionally, even if special care was taken during ROI delineation to avoid including cerebrospinal fluid (CSF) and to maintain consistency in measurements, the use of the ratio to the contralateral region further reduces potential biases from CSF signals, as both the region of interest and its contralateral counterpart are expected to experience similar partial volume effects. The use of sodium ^{23}Na MRI in research and clinical settings requires specialized equipment and optimized pulse sequences. Despite these challenges, advancements in clinical MRI scanner field strengths and the increasing availability of necessary resources support the potential of sodium MRI to offer valuable insights into the evaluation of stroke pathophysiology.

5 | Conclusion

Our findings corroborate those of Hussain et al. [11] and those of Mohamed et al. [22], demonstrating that, at the group level, ^{23}Na signal intensity in humans increases in a time-dependent, sigmoidal manner following the onset of ischemic stroke. In contrast, ADC variations exhibit a more limited dynamic response, reaching a plateau within a few hours post-onset. Regions with ionic edema showed a non-linear increase in ^{23}Na signal during the first 70 h, with faster and larger sodium accumulations in regions progressing to necrosis at month 3 compared to the overall ionic edema. Considering the role of ionic edema imaging in the subacute phase of stroke may provide additional insights into tissue viability and delayed changes in sodium metabolism. Sodium MRI could offer additional information about stroke pathophysiology in the first 70 h. The significant inter-individual heterogeneity observed underscores the need for an individualized approach in future studies.

Acknowledgments

This work was performed by a laboratory member of France Life Imaging network (grant ANR-11-INBS-0006). This work was supported by the ANR grant "NEUROintraSOD-7T" (ANR-15-CE19-0019-01). This work was performed by a laboratory member of the NeuroMarseille Institute funded by the French government under the "France 2030" investment plan managed by the French National Research Agency (reference: ANR-16-CONV000X/ANR-17-EURE-0029) and from Excellence Initiative of Aix Marseille University - A*MIDEX (AMX-19-IET-004).

Conflicts of Interest

The authors declare no conflicts of interest.

Data Availability Statement

The data that support the findings of this study are available from the corresponding author upon reasonable request.

References

1. R. Brouns and P. P. De Deyn, "The Complexity of Neurobiological Processes in Acute Ischemic Stroke," *Clinical Neurology and Neurosurgery* 111, no. 6 (2009): 483–495, https://doi.org/10.1016/j.clineuro.2009.04.001.

2. R. G. González, "Clinical MRI of Acute Ischemic Stroke," *Magnetic Resonance Imaging* 36, no. 2 (2012): 259–271, https://doi.org/10.1002/jmri.23595.

3. M. El-Koussy, G. Schroth, C. Brekenfeld, and M. Arnold, "Imaging of Acute Ischemic Stroke," *European Neurology* 72, no. 5–6 (2014): 309–316, https://doi.org/10.1159/000362719.

4. H. Zeng and Q. Zhu, "Application of Imaging Modalities for Endovascular Thrombectomy of Large Core Infarcts in Clinical Practice,"

Frontiers in Neurology 15 (2024): 1272890, https://doi.org/10.3389/fneur.2024.1272890.

5. P. Vilela and H. A. Rowley, "Brain Ischemia: CT and MRI Techniques in Acute Ischemic Stroke," *European Journal of Radiology* 96 (2017): 162–172, https://doi.org/10.1016/j.ejrad.2017.08.014.

6. M. Goyal, J. M. Ospel, B. Menon, et al., "Challenging the Ischemic Core Concept in Acute Ischemic Stroke Imaging," *Stroke* 51, no. 10 (2020): 3147–3155, https://doi.org/10.1161/STROKEAHA.120.030620.

7. E. Neumaier-Probst, S. Konstandin, J. Ssozi, et al., "A Double-Tuned 1H/23Na Resonator Allows 1H-Guided 23Na-MRI in Ischemic Stroke Patients in One Session," *International Journal of Stroke* 10, no. A100 (2015): 56–61, https://doi.org/10.1111/ijs.12547.

8. K. R. Thulborn, D. Davis, J. Snyder, H. Yonas, and A. Kassam, "Sodium MR Imaging of Acute and Subacute Stroke for Assessment of Tissue Viability," *Neuroimaging Clinics of North America* 15, no. 3 (2005): 639–653, https://doi.org/10.1016/j.nic.2005.08.003.

9. F. Wetterling, E. Chatzikonstantinou, L. Tritschler, et al., "Investigating Potentially Salvageable Penumbra Tissue in an In Vivo Model of Transient Ischemic Stroke Using Sodium, Diffusion, and Perfusion Magnetic Resonance Imaging," *BMC Neuroscience* 17, no. 1 (2016): 82, https://doi.org/10.1186/s12868-016-0316-1.

10. A. Tsang, R. W. Stobbe, N. Asdaghi, et al., "Relationship Between Sodium Intensity and Perfusion Deficits in Acute Ischemic Stroke," *Journal of Magnetic Resonance Imaging* 33, no. 1 (2011): 41–47, https://doi.org/10.1002/jmri.22299.

11. M. S. Hussain, R. W. Stobbe, Y. A. Bhagat, et al., "Sodium Imaging Intensity Increases With Time After Human Ischemic Stroke," *Annals of Neurology* 66, no. 1 (2009): 55–62, https://doi.org/10.1002/ana.21648.

12. G. Stoll, B. Nieswandt, and M. K. Schuhmann, "Ischemia/Reperfusion Injury in Acute Human and Experimental Stroke: Focus on Thrombo-Inflammatory Mechanisms and Treatments," *Neurological Research and Practice* 6 (2024): 57, https://doi.org/10.1186/s42466-024-00355-y.

13. F. C. Ng, L. Churilov, N. Yassi, et al., "Prevalence and Significance of Impaired Microvascular Tissue Reperfusion Despite Macrovascular Angiographic Reperfusion (No-Reflow)," *Neurology* 98, no. 8 (2022): e790–e801, https://doi.org/10.1212/WNL.0000000000013210.

14. A. A. Ballout, D. S. Liebeskind, T. G. Jovin, and S. Najjar, "The Imaging-Neuropathological Gap in Acute Large Vessel Occlusive Stroke," *Stroke* 55, no. 12 (2024): 2909–2920, https://doi.org/10.1161/STROKEAHA.124.047384.

15. J. P. Broderick, O. Adeoye, and J. Elm, "The Evolution of the Modified Rankin Scale and Its Use in Future Stroke Trials," *Stroke* 48, no. 7 (2017): 2007–2012, https://doi.org/10.1161/STROKEAHA.117.017866.

16. H. P. Adams, P. H. Davis, E. C. Leira, et al., "Baseline NIH Stroke Scale Score Strongly Predicts Outcome After Stroke: A Report of the Trial of Org 10172 in Acute Stroke Treatment (TOAST)," *Neurology* 53, no. 1 (1999): 126–131, https://doi.org/10.1212/wnl.53.1.126.

17. A. M. Nagel, F. B. Laun, M. Weber, C. Matthies, W. Semmler, and L. R. Schad, "Sodium MRI Using a Density-Adapted 3D Radial Acquisition Technique," *Magnetic Resonance in Medicine: An Official Journal of the International Society for Magnetic Resonance in Medicine* 62, no. 6 (2009): 1565–1573, https://doi.org/10.1002/mrm.22157.

18. Rician Noise Removal by Non-Local Means Filtering for Low Signal-to-Noise Ratio MRI: Applications to DT-MRI," in *Lecture Notes in Computer Science* (Springer, 2008): 171–179, https://doi.org/10.1007/978-3-540-85990-1_21.

19. L. Machegger, P. Bosque Varela, G. Kuchukhidze, et al., "Quantitative Analysis of Diffusion-Restricted Lesions in a Differential Diagnosis of Status Epilepticus and Acute Ischemic Stroke," *Frontiers in Neurology* 13 (2022): 926381, https://doi.org/10.3389/fneur.2022.926381.

20. N. K. Paschke, W. Neumann, T. Uhrig, et al., "Influence of Gadolinium-Based Contrast Agents on Tissue Sodium Quantification in Sodium Magnetic Resonance Imaging," *Investigative Radiology* 53, no. 9 (2018): 555–562, https://doi.org/10.1097/rli.0000000000000487.

21. Y. Ozsunar, K. Koseoglu, T. A. G. M. Huisman, W. Koroshetz, and A. G. Sorensen, "MRI Measurements of Water Diffusion: Impact of Region of Interest Selection on Ischemic Quantification," *European Journal of Radiology* 51, no. 3 (2004): 195–201, https://doi.org/10.1016/j.ejrad.2003.09.013.

22. S. A. Mohamed, A. Adlung, N. K. Ludwig, et al., "Temporal and Spatial Dynamics of Ischemic Stroke Lesions after Acute Therapy: A Comprehensive Edema Assessment Using Combined 1H- and 23Na-MRI," *Cerebrovascular Diseases* (2024): 1–11, https://doi.org/10.1159/000540162.

23. A. Durukan and T. Tatlisumak, "Acute Ischemic Stroke: Overview of Major Experimental Rodent Models, Pathophysiology, and Therapy of Focal Cerebral Ischemia," *Pharmacology Biochemistry and Behavior.* 87, no. 1 (2007): 179–197, https://doi.org/10.1016/j.pbb.2007.04.015.

24. A. Osa García, S. M. Brambati, A. Desautels, and K. Marcotte, "Timing Stroke: A Review on Stroke Pathophysiology and Its Influence Over Time on Diffusion Measures," *Journal of the Neurological Sciences* 441 (2022): 120377, https://doi.org/10.1016/j.jns.2022.120377.

25. Q. He, Y. Wang, C. Fang, et al., "Advancing Stroke Therapy: A Deep Dive Into Early Phase of Ischemic Stroke and Recanalization," *CNS Neuroscience & Therapeutics* 30, no. 2 (2024): e14634, https://doi.org/10.1111/cns.14634.

26. T. Gasull and A. Arboix, "Molecular Mechanisms and Pathophysiology of Acute Stroke: Recent Advances and Controversies," *CIMB.* 46, no. 4 (2024): 2926–2930, https://doi.org/10.3390/cimb46040182.

27. S. A. Menzies, A. L. Betz, and J. T. Hoff, "Contributions of Ions and Albumin to the Formation and Resolution of Ischemic Brain Edema," *Journal of Neurosurgery* 78, no. 2 (1993): 257–266, https://doi.org/10.3171/jns.1993.78.2.0257.

28. O. Gotoh, T. Asano, T. Koide, and K. Takakura, "Ischemic Brain Edema Following Occlusion of the Middle Cerebral Artery in the Rat. I: The Time Courses of the Brain Water, Sodium and Potassium Contents and Blood-Brain Barrier Permeability to 125I-Albumin," *Stroke* 16, no. 1 (1985): 101–109, https://doi.org/10.1161/01.STR.16.1.101.

29. H. Huang, Y. M. Chen, F. Zhu, et al., "Down-Regulated Na+/K+-ATPase Activity in Ischemic Penumbra After Focal Cerebral Ischemia/Reperfusion in Rats," *International Journal of Clinical and Experimental Pathology* 8, no. 10 (2015): 12708.

30. W. D. Heiss and W. O. Zaro, "Validation of MRI Determination of the Penumbra by PET Measurements in Ischemic Stroke," *Journal of Nuclear Medicine* 58, no. 2 (2017): 187–193, https://doi.org/10.2967/jnumed.116.185975.

31. M. Lu, P. D. Mitsias, J. R. Ewing, et al., "Predicting Final infarct Size Using Acute and Subacute Multiparametric MRI Measurements in Patients With Ischemic Stroke," *Magnetic Resonance Imaging* 21, no. 5 (2005): 495–502, https://doi.org/10.1002/jmri.20313.

32. M. Pérez-Mato, E. López-Arias, A. Bugallo-Casal, et al., "New Perspectives in Neuroprotection for Ischemic Stroke," *Neuroscience* 550 (2024): 30–42, https://doi.org/10.1016/j.neuroscience.2024.02.017.

33. A. Adlung, M. Samartzi, L. R. Schad, E. Neumaier-Probst, M. Fatar, and S. A. Mohamed, "Tissue Sodium Concentration within White Matter Correlates with the Extent of Small Vessel Disease," *Cerebrovascular Diseases* 50, no. 3 (2021): 347–355, https://doi.org/10.1159/000514133.

Supporting Information

Additional supporting information can be found online in the Supporting Information section.